The Astrophysical Journal, 730:13 (9pp), 2011 March 20 doi:10.1088/0004-637X/730/1/13

COSMIC-RAY MODULATION BY THE GLOBAL MERGED INTERACTION REGION IN THE HELIOSHEATH

Xi Luo[1], Ming Zhang[1], Hamid K. Rassoul[1], and N. V. Pogorelov[2]
[1] Department of Physics and Space Sciences, Florida Institute of Technology, 150 West University Boulevard, Melbourne, FL 32901, USA
[2] Department of Physics and Center for Space Plasma and Aeronomic Research, University of Alabama in Huntsville, 301 Sparkman Dr., Huntsville, AL 35899, USA
Received 2010 May 28; accepted 2011 January 14; published 2011 February 24

ABSTRACT

It was found by *Voyager 1* and *Voyager 2* that the Global Merged Interaction Region (GMIR) still has effects on cosmic-ray transport in the heliosheath. The GMIR produced by the intense solar activities of 2005 September propagated into the heliosheath in 2006, causing several decreases in the cosmic-ray flux at *Voyager 1*. Motivated by these observations, we investigate cosmic-ray modulation by the GMIR in the heliosheath using a three-dimensional Galactic cosmic-ray modulation code that includes the drift effect, termination shock, and a propagating GMIR. The simulation reproduces all major modulation features found by previous cosmic-ray observations in the supersonic solar wind region. However, when the simulation is made for the heliosheath region during a passage of the GMIR, the cosmic-ray modulation shows a new feature. The cosmic-ray fluxes at many locations in the heliosheath region experience two distinguished decreases. One coincides with the GMIR's arrival at the termination shock, the other with its arrival at the observing points. Based on this feature, we use the *Voyager* observations of the 2006 GMIR modulation events to derive the radial distance of the termination shock of ∼91 AU and the GMIR shock propagation speed inside the heliosheath of ∼172 km s^{-1} for this event.

Key words: cosmic rays – shock waves – solar wind – Sun: heliosphere

Online-only material: color figures

1. INTRODUCTION

Since the initial establishment of the cosmic-ray transport equation (Parker 1965), much progress has been made in understanding the physics of the cosmic-ray modulation. The important roles of the drift term in the transport equation were realized later (Jokipii et al. 1977; Jokipii & Kopriva 1979). The main features of both the 11 year solar and 22 year hale cycles of cosmic-ray variations were explained using the cosmic-ray drift pattern in the heliospheric magnetic field with a tilted current sheet (Jokipii & Thomas 1981; Kota & Jokipii 1983). However, it appears that some shorter-term cosmic-ray variations must be explained by mechanisms other than drift. One such mechanism is the Global Merged Interaction Region (GMIR), which was introduced by Burlaga et al. (1993). The GMIR is a solar wind structure formed in the inner heliosphere, approximately 5 AU beyond the Sun. It is a build-up of multiple large coronal mass ejections (CMEs) with enhanced solar wind speed and magnetic field. The build-up is powerful enough to survive to very large radial distances despite its interactions with the slower solar wind in front of it. Analyzing the observed cosmic-ray intensity for energy >70 MeV by *Voyager 1* and *Voyager 2*, Burlaga et al. (1985) found that cosmic-ray intensity decreases when a GMIR passes any observation point. The modulation effect of the GMIR can be understood as the effect of a propagating diffusion barrier (Perko & Fisk 1983). When a cosmic-ray particle encounters a GMIR, it is trapped in the GMIR's stronger magnetic field, so it diffuses more slowly and loses more energy. This could cause cosmic-ray intensity to decrease. During the phase of increasing solar activity, GMIRs are formed more frequently and propagate outward in series, leading to long-term depression of cosmic-ray intensity during this phase of solar activity. This scenario has been proposed as an alternative explanation for the 11 year solar cycle variation (McDonald et al. 1993).

Perko & Fisk (1983) studied the effect of diffusion barriers on cosmic-ray propagation and were able to reproduce some basic features seen in short-term cosmic-ray modulation. The true role of the GMIR in the long-term modulation of cosmic ray became clearer when investigators considered the changing tilt angle of the heliospheric current sheet and diffusion barrier during a full solar cycle (Potgieter et al. 1993; Potgieter & Le Roux 1994; Le Roux & Potgieter 1995; Ferreira & Potgieter 2004). It was concluded that GMIR propagations can successfully explain the step-like decrease of cosmic-ray intensity during the ascending phase of solar activity to the solar maximum, while the tilt angle has its major effects during other phases of the solar cycle. The interplay of the GMIR and the current sheet tilt angle as separate dominating factors is essential to explaining the complete 11 year solar cycle of cosmic-ray modulation (Le Roux & Potgieter 1995).

The above findings are mainly confined to the supersonic solar wind region, namely, inside the termination shock region. However, for the cosmic-ray modulation inside the heliosheath, there is still much to be explored (Webber & Lockwood 2001). The *Voyager* observations reveal that the cosmic ray is still modulated by the GMIR at large distances (Burlaga et al. 2003), both inside and outside of the termination shock. For example, it was reported that the $E > 70$ MeV galactic cosmic-ray flux decrease observed by *Voyager 2* in 2006 March is associated with a GMIR arrival at the spacecraft (Webber et al. 2007; Richardson et al. 2006). The same GMIR propagated across the termination shock into the heliosheath and produced the cosmic-ray flux decreases observed by *Voyager 1*. However, the detailed features of cosmic-ray decreases observed by *Voyager 1* in the heliosheath are different from the typical GMIR modulation (Webber et al. 2007) in the supersonic solar wind region. There appear to be several decreases associated with the same GMIR event. Webber et al. (2007, 2009) speculate that one of them was caused by the GMIR when it arrived at the termination shock. This difference motivated us to investigate GMIR modulation effect inside the heliosheath.

In this paper, we solve the cosmic-ray transport equation in a model heliosphere with a GMIR. The heliosphere includes

the following essential features: a supersonic solar wind region with a tilted current sheet; termination shock; a heliosheath region; and a heliopause, which is considered as an interface to the interstellar medium. The GMIR is a propagating diffusion barrier with enhanced solar wind speed. We study how the cosmic-ray flux varies when a GMIR passes through various regions. We particularly look for differences in the modulation of cosmic rays inside the heliosheath and their dependence on model parameters.

2. COSMIC-RAY MODULATION AND THE GMIR MODEL

Our simulation uses Parker's transport equation to study galactic cosmic-ray modulation (Parker 1965):

$$\frac{\partial f}{\partial t} = -(\vec{V}+\langle\vec{v_D}\rangle)\cdot\nabla f+\nabla\cdot(K^{(s)}\cdot\nabla f)+\frac{1}{3}(\nabla\cdot\vec{V})\frac{\partial f}{\partial \ln P} \quad . \quad (1)$$

In this equation, the first term $(\vec{V}+\langle\vec{v_D}\rangle)\cdot\nabla f$ is the solar wind convection plus particle gradient/curvature drift velocities; the second term $\nabla\cdot(K^{(s)}\cdot\nabla f)$ is the diffusion term; and the last term $\frac{1}{3}(\nabla\cdot V)\partial f/\partial \ln P$ is the adiabatic energy change term. In the magnetic field coordinate system, the diffusion tensor $K^{(s)}$ is written as

$$K^{(s)} = \begin{pmatrix} \kappa_\perp & 0 & 0 \\ 0 & \kappa_\perp & 0 \\ 0 & 0 & \kappa_\parallel \end{pmatrix} . \quad (2)$$

Following the Markov stochastic method (Zhang 1999), the transport equation can be changed to the following time-backward stochastic differential equations:

$$d\vec{X} = (\nabla\cdot K^{(s)} - \vec{V} - \langle\vec{v_D}\rangle)ds + \sum_\sigma \vec{\alpha_\sigma} dW_\sigma(s)\,, \quad (3a)$$

$$dP = \frac{1}{3}P(\nabla\cdot V)ds\,. \quad (3b)$$

In the equation above, $dW_\sigma(s)$ is the Wiener process, and it can be generated in each step using a Gaussian distribution random number. This set of equations gives the position and momentum increments for pseudo particles in the phase space $(\vec{X}, p)$.

The diffusion coefficients are given by the following relations:

$$\kappa_\parallel = \kappa_{\parallel 0}\beta\left(\frac{P}{p_0}\right)^{b_\parallel}\left(\frac{B_{\rm eq}}{B}\right)^{a_\parallel}, \quad (4a)$$

$$\kappa_\perp = \kappa_{\perp 0}\beta\left(\frac{P}{p_0}\right)^{b_\perp}\left(\frac{B_{\rm eq}}{B}\right)^{a_\perp}. \quad (4b)$$

Note that P and B are momentum and magnetic field strength, respectively, and β is the ratio of particle speed to the speed of light. The p_0 parameter is a reference momentum (in our case 1 GeV c^{-1}); $B_{\rm eq}$ is the magnetic field strength at the heliospheric equator at 1 AU. The constants $\kappa_{\parallel 0}$ and $\kappa_{\perp 0}$ determine the magnitudes of parallel and perpendicular diffusion coefficients. They are chosen to be 50×10^{20} and 5×10^{20}, respectively, with the unit of cm^2 s^{-1}. The exponents are chosen as $a_{\parallel,\perp} = 0.5$ and $b_{\parallel,\perp} = 1$. The choice of the above diffusion coefficients is somewhat arbitrary, but approximately consistent with the overall modulation level inferred by various observations.

As for solar wind, we have adopted a spherically symmetric model that starts at the Sun with $V_{\rm sw} = 400$ km s^{-1}. An ideal termination shock is placed at $r_{\rm TS} = 92$ AU in our simulation. Outside the termination shock, the solar wind speed decreases according to

$$V_{\rm sw} = 120\times\left(\frac{r_{\rm TS}}{r}\right)^2 \ {\rm km\,s^{-1}}\,. \quad (5)$$

The outer boundary of our simulation is chosen to be 150 AU, associated with the nominal location of the heliopause. This is also the outer boundary where the cosmic ray approaches the interstellar spectrum for which we assume the following form:

$$f_{\rm ism}(p) \propto \left(m_0^2c^2+p^2\right)^{-1.8}/p\,. \quad (6)$$

The interplanetary magnetic field is described by Parker's spiral magnetic field model derived from the above solar wind speed using the frozen-in condition. A wavy current sheet is also included.

In our simulation, the GMIR is described as a partial spherical shell with limited latitude coverage. Figure 1 shows the GMIR model that we have adopted in our simulation. Figure 1(A) shows a snapshot of plasma speed roughly along *Voyager 1*'s direction (35°N) when the GMIR is located at ~60 AU. The GMIR propagates at 508 km s^{-1}. The maximum compression ratio of plasma is 2.25 at peak plasma speed. The particle diffusion coefficient inside the GMIR is chosen to be inversely proportional to the plasma compression ratio, which is shown in Figure 1(B). The GMIR is mainly located near the ecliptic plane. GMIR shock strength weakens as the latitude increases, and it nearly disappears near north and south 40° with respect to the ecliptic plane (Figure 1(C)). Figure 1(D) is a time profile of plasma speed as measured at the point (99 AU, 35°N).

The propagation of a GMIR throughout the heliosphere depends on its detailed dynamic interactions between the background solar wind and the CME ejecta. The details of each GMIR event are unique. Here, we choose to use a model proposed by Whang & Lu (1999). In their model, the GMIR was treated as a strong forward shock. They use a shock interaction model, which takes into account the effects of pick up ions to characterize GMIR propagation speed and shock strength (compression ratio). Figure 2 shows GMIR propagation speed and the shock compression ratio in our whole simulation region. Their solution is confined to the supersonic solar wind region. As for the heliosheath region, we assume that the GMIR shock weakens after interaction with the termination shock and maintains the same shock strength and propagation speed inside the heliosheath region.

3. RESULTS

We first carry out a simulation to investigate the effect of the GMIR on cosmic-ray modulation in the supersonic solar wind region or inside the termination shock. Since previous calculations of GMIR modulation are available and observations in this region are more unambiguous, we use this to verify our simulation model. Based on the same simulation model, we investigate how cosmic-ray fluxes can be modulated as a GMIR propagates in the heliosheath.

3.1. Cosmic-ray Modulation by GMIR Inside the Termination Shock

As a test of our simulation model, we first simulate the cosmic-ray modulation effect caused by a GMIR in the supersonic solar wind region inside the termination shock. The

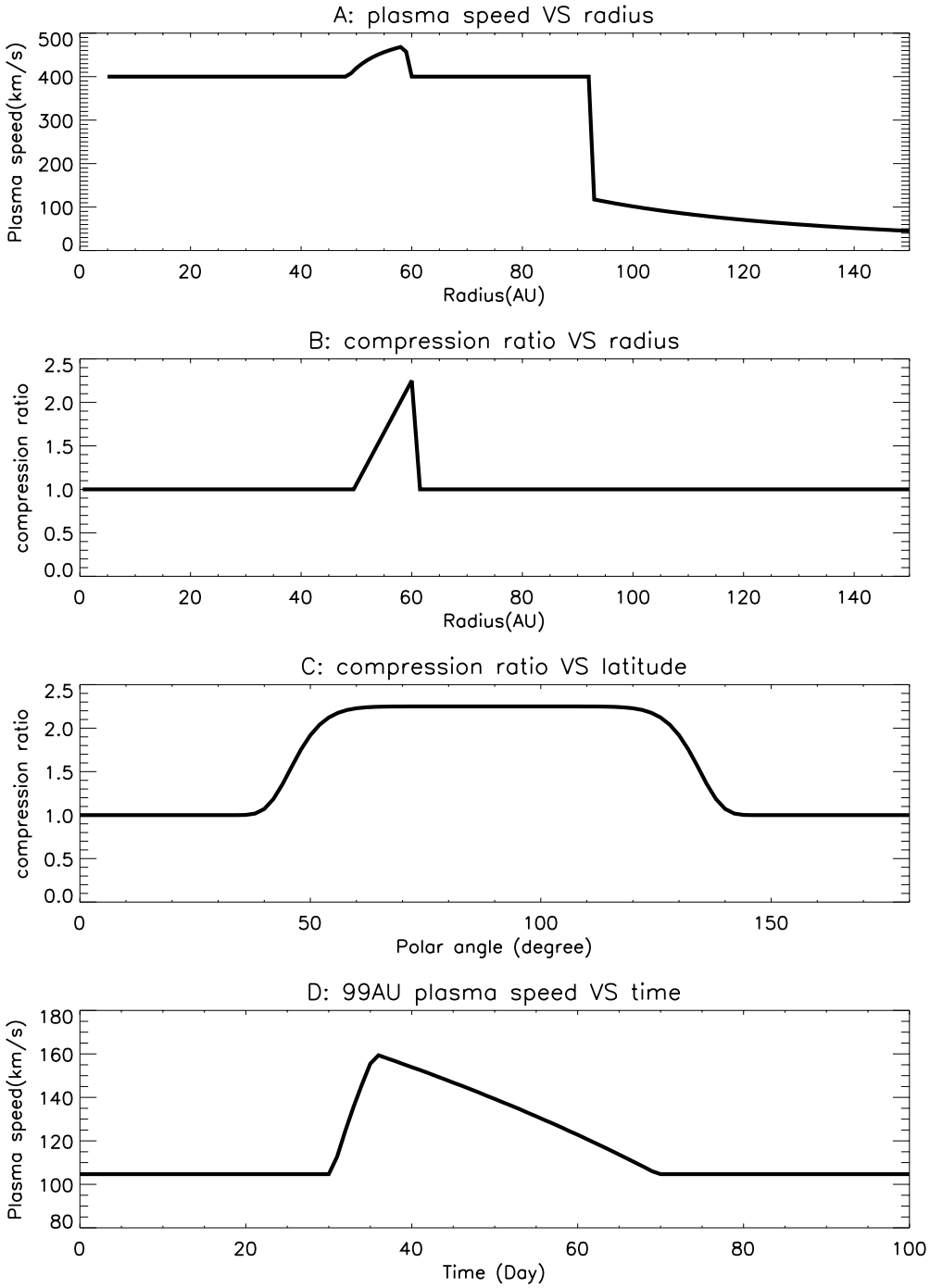

Figure 1. Model of GMIR used in our simulation. The top three panels show a snapshot of plasma speed, plasma compression ratio, and latitudinal distribution of the GMIR shock compression ratio. The bottom panel shows plasma speed as it is measured by an observer at 99 AU in the heliosheath.

result is given in the top panel of Figure 3. It shows the time variation of the 200 MeV cosmic-ray flux at 60 AU radial distance, 35°N heliolatitude (which is approximately along the trajectory of the *Voyager 1* spacecraft). For comparison, the calculated cosmic-ray flux is accompanied by the plasma speed at the same location. The cosmic-ray flux increases slightly before the arrival of the GMIR. This is a sweeping effect of the GMIR, which was also found in a previous simulation (Perko & Fisk 1983). Upon the arrival of the GMIR shock front at the observation point, the cosmic-ray flux begins to decrease. The decrease continues until the GMIR passes the observation point entirely, leaving the cosmic-ray flux at its minimum level. After the GMIR passes, the cosmic-ray flux recovers slowly. The rate of recovery depends on how quickly the cosmic ray can refill the volume swept by the GMIR and how wide a longitude and latitude range the GMIR extends. The entire profile of GMIR modulation of cosmic rays agrees with previous simulations and observations.

3.2. Cosmic-ray Modulation by the GMIR in the Heliosheath

After verifying our simulation model, we turn our attention to cosmic-ray modulation caused by the GMIR in the heliosheath region. The simulation is carried out at the location of 99 AU, 35°N heliolatitude with the same GMIR continuing to propagate

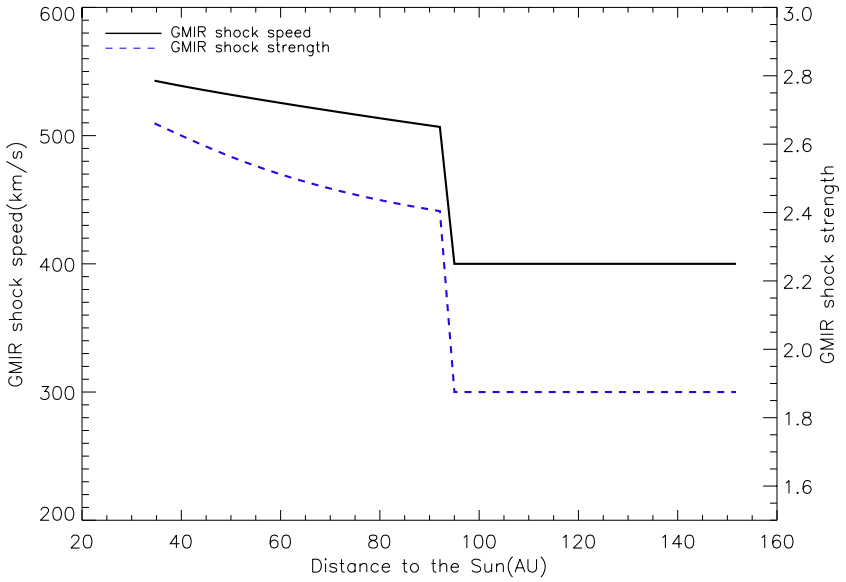

Figure 2. GMIR shock compression ratio (shock strength) and propagation speed as a function of radial distance (obtained from Whang's model). The GMIR shock is assumed to be constant in the heliosheath.

(A color version of this figure is available in the online journal.)

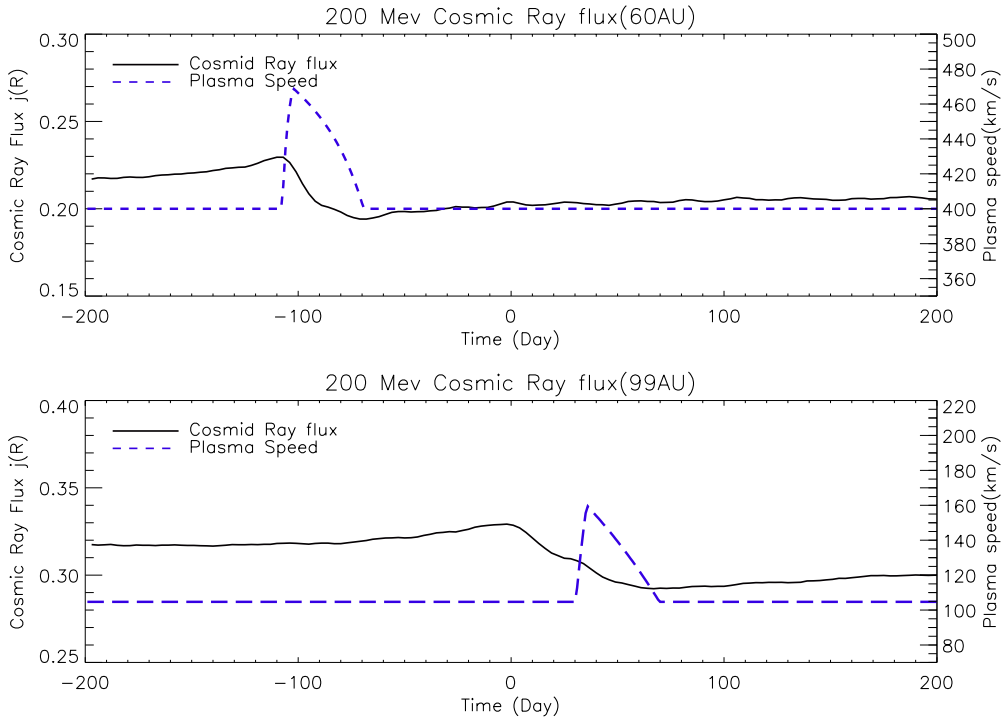

Figure 3. Simulated cosmic-ray flux and plasma speed at 60 AU and 99 AU at 35° N heliolatitude. Time $t = 0$ is set when the GMIR front arrives at the termination shock at $R_{TS} = 92$ AU.

(A color version of this figure is available in the online journal.)

into the heliosheath. The bottom panel of Figure 3 shows the calculated 200 MeV cosmic-ray flux and plasma speed as a function of time. This time profile of the cosmic-ray flux shows a slightly different feature from the one inside the termination shock. The cosmic-ray flux decreases when the GMIR arrives and recovers after the GMIR entirely passes the observation point; however, instead of only one decrease corresponding with the arrival of the GMIR shock, an extra decrease happens before shock arrival at the observation point. This extra decrease corresponds to the time when the GMIR arrives at the termination shock, which we set to occur at $t = 0$. It seems that the cosmic ray observed in the heliosheath can remotely sense GMIR arrival at the termination shock.

Is the feature of cosmic-ray flux decrease upon GMIR arrival at the termination shock a general property of cosmic-ray modulation by the GMIR in the heliosheath? In the following section, we will explore this feature in more detail.

We carry out a series of simulations under different conditions (see Table 1). First, we change observation points along the *Voyager 1* trajectory to determine the cosmic-ray fluxes at three

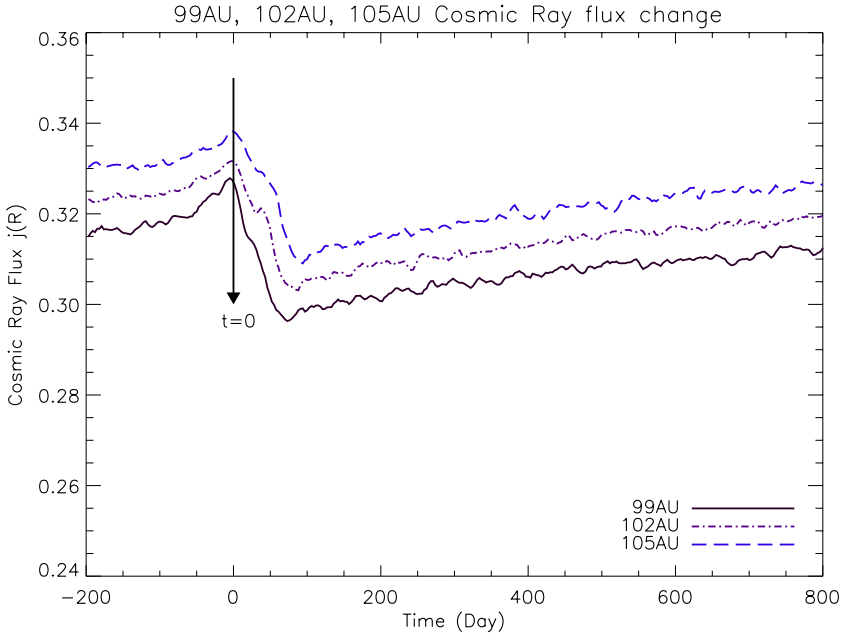

Figure 4. Time variations of the cosmic-ray flux at different locations in the heliosheath. Time $t = 0$ is set when the GMIR front arrives at the termination shock at $R_{TS} = 92$ AU.
(A color version of this figure is available in the online journal.)

Table 1
Parameters Used in Cosmic-Ray Modulation Simulation

Model	Cosmic Ray Energy	Tilt Angle	Observing Radius
1	200 MeV	45	99 AU
2	200 MeV	45	102 AU
3	200 MeV	···	105 AU
4	200 MeV	10	99 AU
5	200 MeV	30	99 AU
6	200 MeV	···	99 AU
7	400 MeV	···	···
8	1 GeV	···	···

Table 2
Gradient of the Cosmic-ray Flux Curve for 200 MeV

Time	Flux Value(99 AU)	Derivative with Respect to Time
−20.0	0.326672	0.000569972222
−17.0	0.327533	0.000217361111
−14.0	0.328145	0.000173388889
−11.0	0.328573	9.08611111E-05
−8.0	0.32875	9.16944444E-05
−5.0	0.329102	4.79722222E-05
−2.0	0.329076	0.000122277778
1.0	0.329454	−0.000298861111
4.0	0.327164	−0.000879416667
7.0	0.324565	−0.000905138889
10.0	0.321623	−0.00118805556
13.0	0.317711	−0.00113002778
16.0	0.315102	−0.000702694444
19.0	0.313078	−0.000968055556
22.0	0.309856	−0.00036975
25.0	0.310593	−0.000182083333

different radial distances: 99 AU, 102 AU, and 105 AU, all at 35°N heliolatitude. Second, we investigate the effect caused by changing tilt angles, which represent different periods of solar activity. Finally, we study how cosmic-ray modulation by the GMIR looks at different energies of cosmic ray. We find that the feature of the cosmic-ray remotely sensing GMIR arrival at the termination shock appears in all these simulations.

3.2.1. The GMIR Modulation Effect in the Heliosheath for Different Locations

Figure 4 shows the time variation of the cosmic-ray flux as the GMIR propagates in the heliosheath. The results of 99 AU, 102 AU, and 105 AU are illustrated by the black, brown, and blue lines, respectively. The tilt angle of the current sheet is set at 45° in these simulations, which results in a small but visible solar rotational variation of the cosmic-ray flux. This is a small variation compared to the cosmic-ray variation caused by a GMIR and is not the target of our investigation here. In all these curves, there are two major decrease events; the first decrease is always at $t = 0$, or the time when the GMIR arrives at the termination shock. In order to quantitatively identify the trend of the cosmic-ray flux and find the starting times of the decrease events, we calculate the time derivative of these flux curves near the turning point. If the sign of derivatives changes from positive to negative, it means the curve is beginning to decrease.

Table 2 shows the time derivative of the flux curve (day^{-1}) near the turning point for the calculated cosmic-ray flux at 99 AU with an ad hoc GMIR propagation. It is clear that around $t = 0$, the time derivative changes sign from a positive to a negative value, indicating that the cosmic-ray flux begins to decrease amid an uptrend generally seen long before the GMIR. At $t = 0$, the GMIR shock is still at the location of the termination shock, or 92 AU away from the Sun in our simulation. The cosmic ray at some point even 7 AU downstream of the termination can sense GMIR arrival at the termination shock. We refer to this feature as the "remote sensing capability of cosmic rays."

In the same plot, we find that the second decrease begins about $t = 30$ for the cosmic-ray flux at 99 AU. After comparing

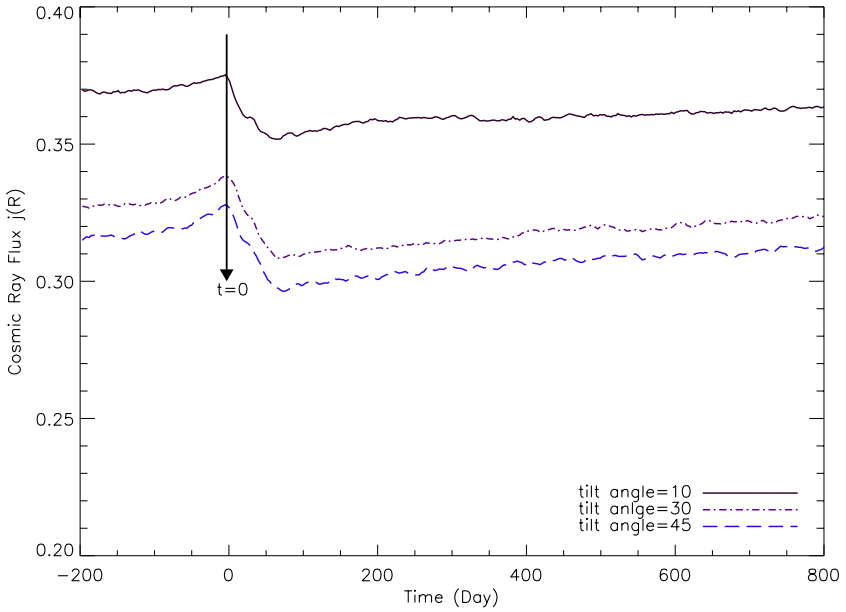

Figure 5. Time variations of the cosmic-ray flux caused by a GMIR in the heliosheath for different current sheet tilt angles.
(A color version of this figure is available in the online journal.)

with the plasma speed plot at this location, we find that it coincides with the time when the GMIR shock front arrives at the observation point.

The time variations of the cosmic-ray fluxes at 102 AU and 105 AU are also drawn in Figure 4. The cosmic ray starts with a higher flux as the observation point goes further out. This is consistent with a positive radial gradient expected considering the fact that the cosmic ray comes from the interstellar medium outside of the heliosphere. Cosmic-ray fluxes at all three radial distances begin to decrease at $t = 0$, when the GMIR arrives at the termination shock. Then the rate of flux decrease becomes smaller and the fluxes at 102 AU and 105 AU even form small plateaus. It seems that the amount of flux decrease from the flux peak at $t = 0$ to the plateau becomes smaller at a larger distance, indicating the weakening of remote sensing capability when an observer moves away to the termination shock. There is a second decrease in each of the curves at a later time when the GMIR arrives. The second decrease at 102 AU begins around $t = 43$, while it begins around $t = 56$ at 105 AU. The delay is consistent with the time needed for the GMIR shock front to propagate over the additional radial distance in the heliosheath. After the GMIR passes the observation point, the cosmic-ray flux begins to recover. The starting times of cosmic-ray recovery show delay with radial distance, again consistent with radial propagation of the GMIR.

3.2.2. The GMIR Modulation Effect in the Heliosheath for Different Solar Activity Conditions

Figure 5 illustrates the time variation of the cosmic-ray flux at 99 AU, 35°N heliolatitude in different solar activity periods. In our simulation, we use the tilt angle to represent different time periods of solar activity. The top curve is the time variation of the cosmic-ray flux when the tilt angle is set to 10°. This represents a solar minimum condition, when the cosmic-ray modulation is small. The lower two plots correspond to the conditions of tilt angles of 30° and 45°, which correspond to medium levels of solar activity. Clearly, the cosmic-ray flux becomes smaller during these medium solar activity periods. In all these calculations, the cosmic-ray flux begins to decrease when the GMIR arrives at the termination shock, which is followed by the second decrease when the GMIR arrives at the observation point. The relative decrease level in each of the two stages seems to be slightly different for the 10° tilt than that for higher tilt angles. For the small 10° tilt, cosmic-ray modulation by the GMIR is more sensitive to GMIR arrival at the termination shock than to modulation produced by the GMIR arriving locally.

3.2.3. The GMIR Modulation Effect in the Heliosheath for Different Energies

Finally, we simulated cosmic-ray modulation by the GMIR in the heliosheath for particles with three different energies, 200 MeV, 400 MeV, and 1 GeV. Figure 6 illustrates these results. The effect of cosmic-ray modulation by the GMIR with two stages of flux decrease is clearly visible at all three energies. Compared with the GMIR modulation of 200 MeV cosmic rays, the 400 MeV and 1 GeV cosmic-ray fluxes are modulated less by the GMIR due to a larger diffusion coefficient at higher energies, while the 27 day solar rotation variation at these two higher energies becomes stronger. Even so, we can see that the cosmic-ray flux begins to decrease long before the GMIR's local arrival. The 400 MeV cosmic-ray flux begins to decrease even before GMIR arrival at the termination shock at $t = 0$, but given the magnitude of the 27 day variation it is hard to say if this earlier arrival is real or not. For the 1 GeV cosmic-ray flux, the earlier decrease is more obscure. This indicates that the GMIR has a stronger influence for lower energy cosmic-ray particles compared with higher energy cosmic-ray particles.

4. COMPARISON WITH THE *VOYAGER* OBSERVATIONS

In 2006 March, *Voyager 2* was at 79 AU, 26°S heliolatitude. The flux of $E > 70$ MeV Galactic cosmic rays at *Voyager 2* shows a strong decrease beginning at 2006.19 (Figure 7). It is accompanied by a jump in solar wind speed and density. These observations give strong evidence that the cosmic-ray flux decrease in 2006.19 is the result of a GMIR shock's arrival at the *Voyager 2* location (Richardson et al. 2006), as the details of

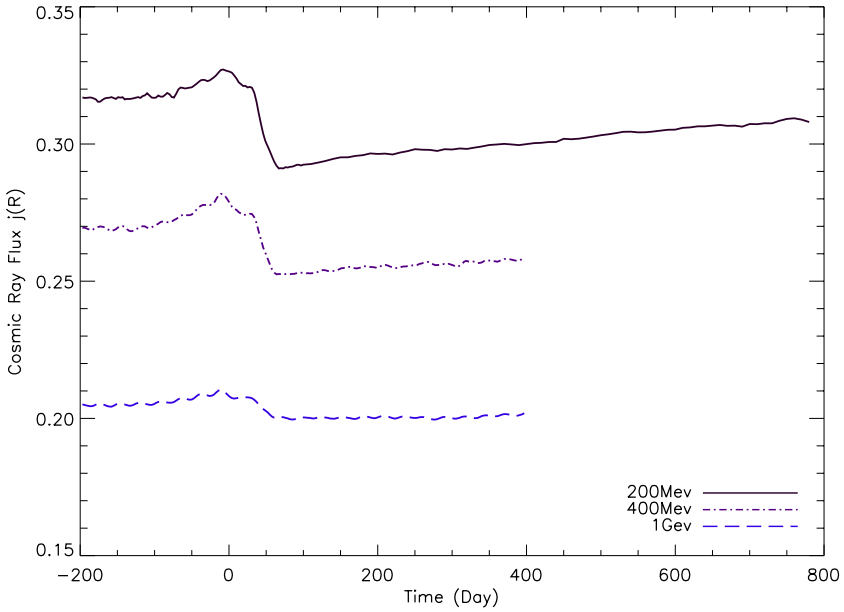

Figure 6. Time variations of GMIR modulation on cosmic rays of three different energies.
(A color version of this figure is available in the online journal.)

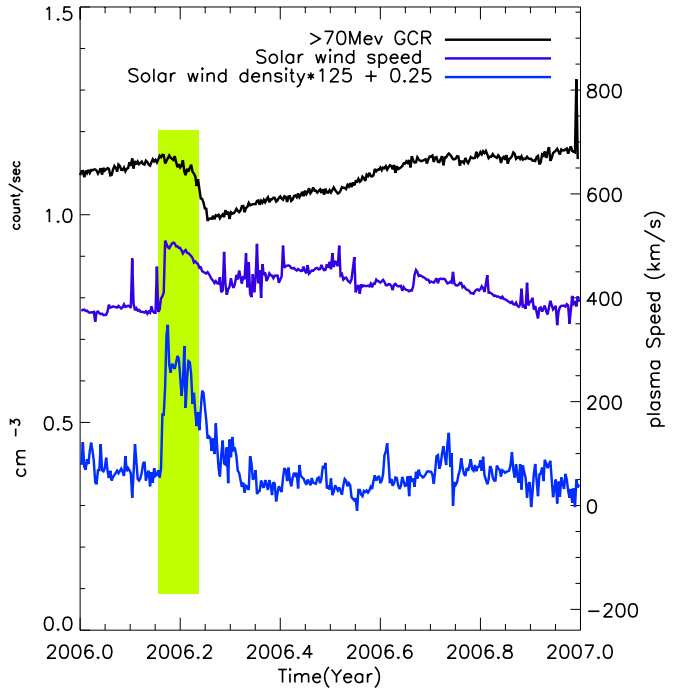

Figure 7. *Voyager 2* measurements of plasma speed, density, and cosmic-ray intensity in 2006 when a GMIR passed the spacecraft.
(A color version of this figure is available in the online journal.)

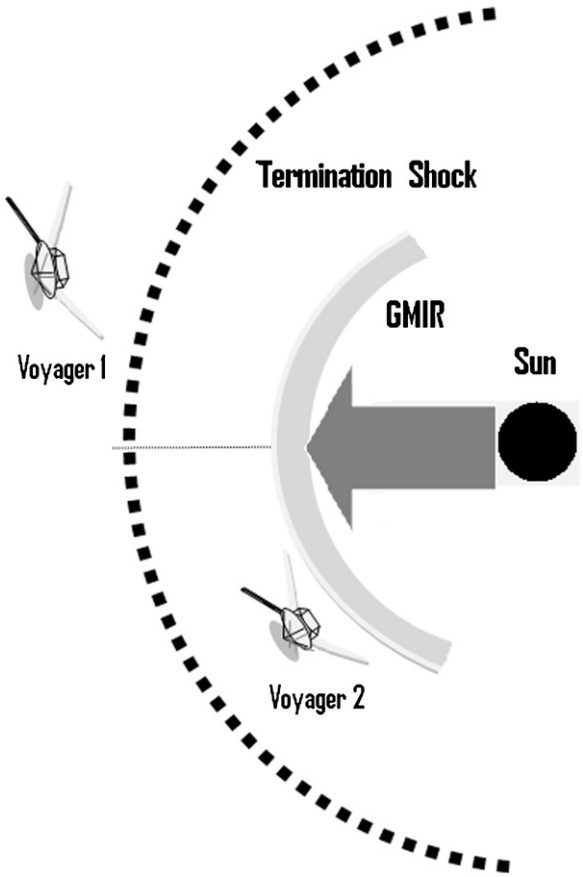

Figure 8. Illustration of *Voyager 2* and *Voyager 1* location with respect to termination shock in the heliosphere.

the cosmic-ray flux and solar wind variations obey the profile of a typical GMIR in the supersonic solar wind region. This GMIR is probably associated with the high solar activities occurring in 2005 September.

As suggested by Webber et al. (2007), the same GMIR propagated further out to *Voyager 1* at 99 AU, 34°N heliolatitude, which at that time was in the heliosheath. In Figure 8, we illustrate the two *Voyagers*' locations with respect to the termination shock. In addition, a GMIR shock is plotted in the same figure. The cosmic-ray instrument on *Voyager 1* at 99 AU, 34°N heliolatitude detected two cosmic-ray flux decrease events, one happening around 2006.29 and the second around 2006.51 (Figure 9). If we assume that the first decrease is associated with the GMIR shock arriving at *Voyager 1*'s location, then the estimated GMIR shock propagation speed will be so large as

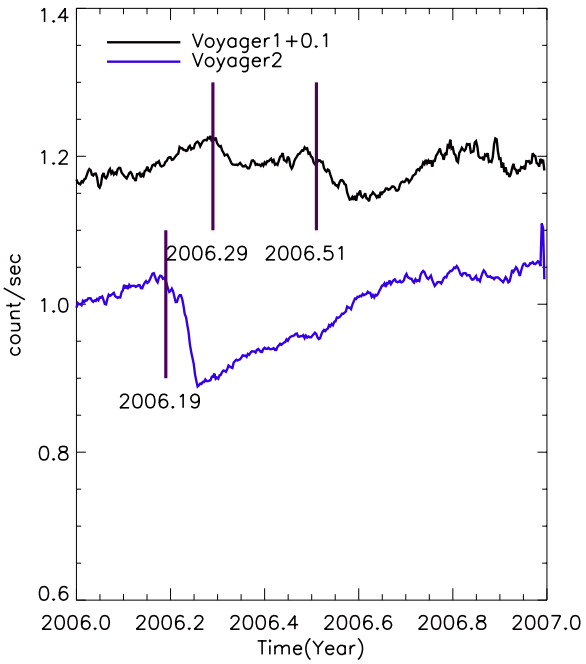

Figure 9. Comparison of $E > 70$ MeV Galactic cosmic-ray measurements by *Voyager 2* in the supersonic solar wind and *Voyager 1* in the heliosheath.
(A color version of this figure is available in the online journal.)

to be unreasonable (Webber et al. 2009). The only reasonable explanation is that the first decrease of the cosmic-ray flux was caused by the GMIR shock arrival at the termination shock. This is consistent with the remote sensing feature of cosmic rays found in our simulation.

Webber et al. (2007) also attributed another transient decrease of the cosmic ray observed by *Voyager 1* at 2006.89 for the arrival of the same GMIR at the heliopause. However, we have not yet found this effect in our simulation. It is probably because the interaction between the GMIR shock and the heliopause has been removed in our simulation, since the heliopause is the outer boundary of our model. In future model runs, we will move the outer boundary of our model to a larger radial distance to further explore this effect.

5. APPLICATION OF THE COSMIC-RAY REMOTE SENSING FEATURE

The feature of cosmic-ray flux decrease at the time of GMIR arrival at the termination shock appears in nearly all of our simulation results within the heliosheath region. From our simulations, this feature can be seen in the heliosheath even farther than 13 AU downstream of the termination shock. This gives us a new way to detect the location of the termination shock with remote cosmic-ray measurement in the heliosheath.

As an example, let us now use the 2006 GMIR event to locate the termination shock at that time. The process requires the propagation speed of the GMIR between GMIR arrival at the termination shock and at either one of the *Voyager* spacecrafts to be known. Since the plasma instrument on *Voyager 1* is not working, we can only rely on the *Voyager 2* plasma data to calculate GMIR shock propagation speed in the supersonic solar wind. We assume that the GMIR propagates at the same speed at the southern heliolatitude of *Voyager 2* and the northern heliolatitude of *Voyager 1*. *Voyager 2* detected the GMIR shock at the time 2006.19 and location 79 AU, 27°S heliolatitude. The background solar wind density and speed were $n_1 = 0.0011$ cm^{-3}, $V_1 = 380$ km s^{-1}. Immediately after the shock passage, the solar wind density and speed were $n_2 = 0.0032$ cm^{-3} and $V_2 = 506$ km s^{-1}. Using the Rankine–Hugoniot relationship of shock compression,

$$\frac{n_1}{n_2} = \frac{V_{\rm GMIR} - V_2}{V_{\rm GMIR} - V_1} \quad , \tag{9}$$

we can obtain the propagation speed of the GMIR shock $V_{\rm GMIR} \approx 572$ km s^{-1}. There is no reason to suspect that the speed would substantially change between *Voyager 2*'s location and the termination shock. The time of GMIR arrival at the termination shock location was 2006.29. The GMIR shock takes 2006.29–2006.19 = 0.1 yr traveling from *Voyager 2* (79 AU) to the termination shock. Using GMIR shock velocity and travel time, we determine the radial distance between *Voyager 2* (79 AU) and the location of the termination shock to be about 12 AU. Thus, the termination shock should be located at a radial distance $R_{\rm TS} \approx 91$ AU along *Voyager 1*'s direction in 2006 March. The termination shock had moved in since the first crossing by *Voyager 1* in 2004 December at 94 AU (Stone et al. 2005). Compared with the termination shock crossing by *Voyager 2* in 2007 September at 84 AU (Stone et al. 2008), the termination shock is still a little farther out. It is possible that the termination shock could have continued to move in since 2006, but the difference could also come from the possibility that the termination shock is not spherically symmetric.

In addition to the capability of calculating the location of termination shock, we can also estimate the shock propagation speed in the heliosheath. Based on *Voyager 1*'s cosmic-ray measurement, we know that the GMIR shock traveled from the termination shock (91 AU) to *Voyager 1*'s location (99 AU) from 2006.29 to 2006.51. Thus, the propagation speed of GMIR can be obtained: $V_{\rm sheath} \approx 172$ km s^{-1}.

After obtaining these estimated values about the GMIR event, we have an opportunity to compare our simulation result with the *Voyager 1* data directly. This comparison is shown in Figure 10. In the simulation, we set the reduced GMIR propagation speed in the heliosheath to 172 km s^{-1} and the termination shock radial distance to 91 AU. In addition, the compression ratio of GMIR inside termination shock follows: $n_2/n_1 \approx 2.9$. Our simulation does correctly predict the onset times of these two decreases found in the *Voyager 1* cosmic-ray flux data.

6. DISCUSSION AND SUMMARY

We have presented our simulation results of cosmic-ray modulation of a propagating GMIR in the heliosphere. It is based on a stochastic simulation method to solve the Parker transport equation. Then we have applied the result of our calculation to observations made by the *Voyager* spacecrafts.

Our calculation reproduces the previously found major features of cosmic-ray modulation by GMIR propagation within the supersonic solar wind region. The cosmic-ray flux slightly increases before a GMIR arrives at the observation point, meaning cosmic rays are piled up before GMIR arrival. When the GMIR front arrives, the cosmic-ray flux will decrease until the entire GMIR passes, followed by a slow recovery.

In the heliosheath, the local effect of GMIR modulation of cosmic rays shows the same major feature as in the supersonic solar wind region, except that the magnitude of local GMIR modulation is slightly smaller due to weakening of GMIR shock strength. However, there is an additional feature of the GMIR modulation in the heliosheath. The cosmic-ray flux begins to

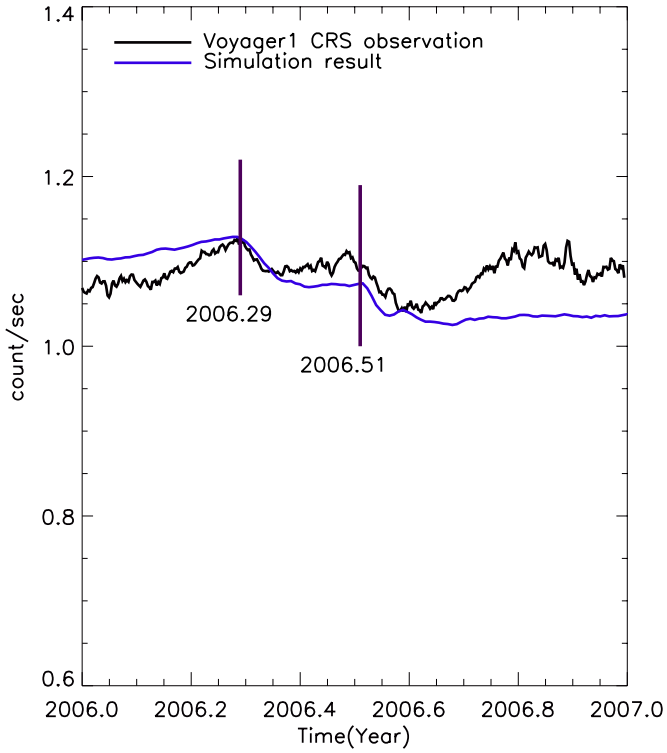

Figure 10. Comparison between *Voyager 1* measurement of $E > 70$ MeV Galactic cosmic-ray intensity and our model calculation. Two lines indicate the beginning time of cosmic-ray decreases.

(A color version of this figure is available in the online journal.)

decrease when the GMIR arrives at the termination shock, resulting in two stages of cosmic-ray decrease. This feature should arise from the fact that cosmic-ray transport in the heliosphere is a random walk process. The cosmic-ray particle may go through the termination shock and tour vast regions of the supersonic solar wind region before it is detected inside the heliosheath. Our simulation shows that a cosmic-ray particle at V1 location (99 AU, 55°N) has spent about 329 days inside the termination shock and 508 days inside the heliosheath. This value is obtained by averaging 100,000 test particles' history in our simulation. Similar concepts have previously been demonstrated (Florinski & Pogorelov 2009; Ball et al. 2005). Although the energy change term is small in the heliosheath, cosmic-ray particles detected inside the heliosheath have already spent much time inside the termination shock, where the cooling is significant. Cosmic rays in the heliosheath are still modulated by the solar wind.

The GMIR effect on cosmic rays is a result of competition among several processes. Whether the cosmic-ray flux increases or decreases at a location near a GMIR (even in the supersonic solar wind) depends on the levels of effectiveness of the following four physical processes: trapping or barricading by the reduced diffusion inside the GMIR, enhanced adiabatic cooling behind the GMIR, a sweeping effect in front of the GMIR (gradient of diffusion coefficient), and acceleration by GMIR shock compression. These effects are not necessarily local and simultaneous. Thus, no single, isolated physical process causes this remote feature. One possible contribution is that the GMIR can disrupt cosmic-ray acceleration by the termination shock. Another possibility comes from the fact that the GMIR and its effects on particle transport processes in the supersonic solar wind are stronger than in the heliosheath. To an observer in the heliosheath, the strongest and closest GMIR modulation effect occurs when the GMIR arrives at the termination shock. The remote modulation effect overcomes the effects that would cause the cosmic ray to increase before the GMIR's arrival. The cosmic-ray flux decreases earlier as a result of the net effect.

Based on the remote sensing feature we have found in this paper, we have also proposed a method to detect the location of the termination shock using remote cosmic-ray measurement in the heliosheath with the aid of a plasma measurement. When it was applied to *Voyager* observation of the GMIR in 2006 March, we found that the termination shock was located approximately at 91 AU at that time, and the GMIR propagated at a speed of 172 km s^{-1} in the heliosheath.

We thank Edward Stone and John Richardson for their permission to use the *Voyager* cosmic-ray and plasma data. Xi Luo thanks Ismael Diaz for his valuable comments on this paper. This work was supported in part by NASA under grants NNX09AG29G and NNX09AB24G.

REFERENCES

Ball, B., Zhang, M., Rassoul, H., & Linde, T. 2005, ApJ, 634, 1116
Burlaga, L. F., McDonald, F. B., Goldstein, M. L., & Lazarus, A. J. 1985, J. Geophys. Res., 90, 12027
Burlaga, L. F., McDonald, F. B., & Ness, N. F. 1993, J. Geophys. Res., 98, 1
Burlaga, L. F., Ness, N. F., McDonald, F. B., Richardson, J. D., & Wang, C. 2003, ApJ, 582, 540
Ferreira, S. E. S, & Potgieter, M. S. 2004, ApJ, 603, 744
Florinski, V., & Pogorelov, N. V. 2009, ApJ, 701, 642
Jokipii, J. R., & Kopriva, D. A. 1979, ApJ, 234, 384
Jokipii, J. R., Levy, E. H., & Hubbard, W. B. 1977, ApJ, 213, 861
Jokipii, J. R., & Thomas, B. 1981, ApJ, 243, 1115
Kota, J., & Jokipii, J. R. 1983, ApJ, 265, 573
Le Roux, J. A., & Potgieter, M. S. 1995, ApJ, 442, 847
McDonald, F. B., Lal, N., & McGuire, R. E. 1993, J. Geophys. Res., 98, 1243
Parker, E. N. 1965, Planet. Space Sci., 13, 9
Perko, J. S., & Fisk, L. A. 1983, J. Geophys. Res., 88, 9033
Potgieter, M. S., & Le Roux, J. A. 1994, ApJ, 423, 817
Potgieter, M. S., Le Roux, J. A., Burlaga, L. F., & McDonald, F. B. 1993, ApJ, 403, 760
Richardson, J. D., et al. 2006, Geophys. Res. Lett., 33, L23107
Stone, E. C., Cummings, A. C., McDonald, F. B., Heikkila, B. C., Lal, N., & Webber, W. R. 2005, Science, 309, 2017
Stone, E. C., Cummings, A. C., McDonald, F. B., Heikkila, B. C., Lal, N., & Webber, W. R. 2008, Nature, 454, 71
Webber, W. R., Cummings, A. C., McDonald, F. B., Stone, E. C., Heikkila, B., & Lal, N. 2007, Geophys. Res. Lett., 34, L20107
Webber, W. R., Cummings, A. C., McDonald, F. B., Stone, E. C., Heikkila, B. C., & Lal, N. 2009, J. Geophys. Res., 114, A07108
Webber, W. R., & Lockwood, J. A. 2001, J. Geophys. Res., 29333, 106, A12
Whang, Y. C., & Lu, J. Y. 1999, J. Geophys. Res., 104, 19787
Zhang, M. 1999, ApJ, 513, 409